DOI: 10.1021/ic901432j

Inorganic Chemistry
Article

Isolation, Characterization, and Computational Studies of the Novel $[Mo_3(\mu_3\text{-}Br)_2(\mu\text{-}Br)_3Br_6]^{2-}$ Cluster Anion

Patrina Paraskevopoulou,*,† Christodoulos Makedonas,† Nikolaos Psaroudakis,† Christiana A. Mitsopoulou,† Georgios Floros,† Andriana Seressioti,† Marinos Ioannou,† Yiannis Sanakis,‡ Nigam Rath,§ Carlos J. Gómez García,∥ Pericles Stavropoulos,⊥ and Konstantinos Mertis*,†

†*Faculty of Chemistry, University of Athens, Athens 15771, Greece,* ‡*Institute of Materials Science, NCSR "Demokritos", Ag. Paraskevi 15310, Greece,* §*Department of Chemistry and Biochemistry, University of Missouri-St. Louis, St. Louis, Missouri 63121,* ∥*Institute of Molecular Science, University of Valencia, Scientific Park, 46980 Paterna, Spain, and* ⊥*Department of Chemistry, Missouri University of Science & Technology, Rolla, Missouri 65409*

Received July 21, 2009

The novel trimolybdenum cluster $[Mo_3(\mu_3\text{-}Br)_2(\mu\text{-}Br)_3Br_6]^{2-}$ (**1**, $\{Mo_3\}^{9+}$, 9 d-electrons) has been isolated from the reaction of $[Mo(CO)_6]$ with 1,2-$C_2H_4Br_2$ in refluxing PhCl. The compound has been characterized in solution by electrospray ionization mass spectrometry (ESI-MS), UV−vis spectroscopy, cyclic voltammetry, and in the solid state by X-ray analysis (counter-cations: $(n\text{-}Bu)_4N^+$ (**1**), Et_4N^+, Et_3BzN^+), electron paramagnetic resonance (EPR), magnetic susceptibility measurements, and infrared spectroscopy. The least disordered $(n\text{-}Bu)_4N^+$ salt crystallizes in the monoclinic space group *C*2/*c*, $a = 20.077(2)$ Å, $b = 11.8638(11)$ Å, $c = 22.521(2)$ Å, $\alpha = 90$ deg, $\beta = 109.348(4)$ deg, $\gamma = 90$ deg, $V = 5061.3(9)$ Å^3, $Z = 4$ and contains an isosceles triangular metal arrangement, which is capped by two bromine ligands. Each edge of the triangle is bridged by bromine ions. The structure is completed by six terminal bromine ligands. According to the magnetic measurements and the EPR spectrum the trimetallic core possesses one unpaired electron. Electrochemical data show that oxidation by one electron of **1** is reversible, thus proceeding with retention of the trimetallic core, while the reduction is irreversible. The effective magnetic moment of **1** (μ_{eff}, 1.55 μ_B, r.t.) is lower than the spin-only value (1.73 μ_B) for $S = 1/2$ systems, most likely because of high spin−orbit coupling of Mo(III) and/or magnetic coupling throughout the lattice. The ground electronic state of **1** was studied using density functional theory techniques under the broken symmetry formalism. The ground state is predicted to exhibit strong antiferromagnetic coupling between the three molybdenum atoms of the core. Moreover, our calculated data predict two broken symmetry states that differ only by 0.4 kcal/mol (121 cm^{-1}). The antiferromagnetic character is delocalized over three magnetic orbitals populated by three electrons. The assignment of the infrared spectra is also provided.

Introduction

Polynuclear metal−metal bonded complexes of the transition metals are of interest for fundamental reasons, but also for their significance in bioinorganic chemistry, catalysis, and connection with potential applications including metal surfaces, electronic and magnetic devices.[1]

Trimolybdenum compounds usually feature an equilateral (or nearly equilateral) trimetallic core, and depending on ligation, they are categorized in three general classes: (i) the monocapped $[Mo_3X_{13}]$ clusters, which contain six Mo−Mo bonding electrons (Mo−Mo single bond), but can also accommodate one or two more electrons in an orbital that has little, if any, M−M antibonding character, therefore bearing the $\{Mo_3\}^{n+}$ (n = 12−10) cores, for example, $[Mo_3(\mu_3\text{-}S)(\mu\text{-}S)_3(CN)_9]^{5-}$;[2] (ii) the bicapped $[Mo_3X_{17}]$ clusters with $\{Mo_3\}^{n+}$ (n = 12−14) cores and Mo−Mo formal

*To whom correspondence should be addressed. E-mail: cmertis@chem.uoa.gr (K.M.), paraskevopoulou@chem.uoa.gr (P.P.).

(1) (a) *Multiple Bonds Between Metal Atoms*, 3rd ed.; Cotton, F. A., Walton, R. A., Eds.; Springer Science and Business Media: New York, 2005. (b) Holm, R. H.; Kennepohl, P.; Solomon, E. I. *Chem. Rev.* **1996**, *96*, 2239–2314. (c) *Catalysis by Di- and Polynuclear Metal Cluster Complexes*; Adams, R. D., Cotton, F. A., Eds.; Wiley VCH: New York, 1999. (d) Alexeev, O. S.; Gates, B. C. *Ind. Eng. Chem. Res.* **2003**, *42*, 1571–1587.

(2) (a) Howlader, N. C.; Haight, G. P., Jr.; Hambley, T. W.; Lawrance, G. A.; Rahmoeller, K. M.; Snow, M. R. *Aust. J. Chem.* **1983**, *36*, 377–383. (b) Müller, A.; Jostes, R.; Eltzner, W.; Nie, C.; Diemann, E.; Boegge, H.; Zimmermann, M.; Dartmann, M.; Reinsch-Vogell, U. *Inorg. Chem.* **1985**, *24*, 2872–2873.

(3) (a) Bino, A.; Ardon, M.; Maor, I.; Kaftory, M.; Dori, Z. *J. Am. Chem. Soc.* **1976**, *98*, 7093–7095. (b) Bino, A.; Cotton, F. A.; Dori, Z. *J. Am. Chem. Soc.* **1981**, *103*, 243–244. (c) Bino, A.; Cotton, F. A.; Dori, Z.; Kolthammer, B. W. S. *J. Am. Chem. Soc.* **1981**, *103*, 5779–5784. (d) Ardon, M.; Bino, A.; Cotton, F. A.; Dori, Z.; Kaftory, M.; Kolthammer, B. W. S.; Kapon, M.; Reisner, G. *Inorg. Chem.* **1981**, *20*, 4083–4090.

Published on Web 02/04/2010

bond orders of 1, $^5/_6$, and $^2/_3$, respectively, with characteristic members being the series $[Mo_3(\mu_3\text{-}O)_n(\mu_3\text{-}CMe)_{2-n}(O_2CMe)_6(H_2O)_3]^{m+}$ ($n = 0, 2, m = 2$; $n = 1, m = 1$);[3] and (iii) the bicapped $[Mo_3X_{11}]$ clusters, which may be considered to involve $\{Mo_3\}^{n+}$ ($n = 10, 12$) cores, for example, $[Mo_3(\mu_3\text{-}O)(\mu_3\text{-}OR)(\mu\text{-}OR)_3(OR)_6]$ (R = ^{i}Pr, CH_2CMe_3).[4] However, despite the abundance of the aforementioned clusters, very little is known about the bicapped triangulo perhaloderivatives $[Mo_3(\mu_3\text{-}X)_2(\mu\text{-}X)_3X_6]^{2-}$ (X = Cl, Br, I), although their existence is not unprecedented. The chloride has been mentioned,[5] but no details have been reported, and the iodide has been very poorly characterized.[6,7] Their closest known analogues are compounds $[Mo_3(\mu_3\text{-}H)(\mu_3\text{-}I)(\mu\text{-}I)_3I_3L_3]$ (L = THF, MeCN, PhCN),[8] obtained in 6% yield maximum, and $[Mo_3(\mu_3\text{-}O)(\mu_3\text{-}Cl)(\mu\text{-}Cl)_3Cl_6]^{2-}$.[9] In contrast, the $[Mo_3X_{12}]^{3-}$ clusters ($\{Mo_3\}^{9+}$; X = Cl,[10,11] Br,[7,11] I[7,11]) adopt a linear face-sharing trioctahedral structure.

Triangulo metal clusters with alkylidyne (≡CR) ligands are often used as models for the interaction between metal surfaces and organic moieties,[12] but mechanistic investigations of such reactions have been hindered by their complex nature. Homogeneously, the interaction of alkynes with metal−metal bonded complexes can give impressively facile, although rare, multielectron redox reactions, such as: (i) formation of alkylidynes via a six-electron reductive cleavage of an alkyne's triple bond in a metathesis M≡M/C≡C type reaction, as pioneered by Schrock et al.[13] (eq 1); and (ii) alkyne formation via six-electron oxidative alkylidyne coupling, encountered in the room temperature aerobic oxidation of the $\{Mo_3\}^{14+}$ complex ion $[Mo_3(\mu_3\text{-}CMe)_2(\mu\text{-}O_2CMe)_6(H_2O)_3]^{2+}$, as reported recently by Bino et al.[14] In aqueous media 2-butyne is ejected (eq 2), whereas in acidic media (0.8 M HBr) the alkyne formed remains coordinated in a $\mu_3\text{-}\eta_2(\perp)$ fashion in compound $[Mo_3Br_7(\mu\text{-}O_2CMe)(H_2O)_2(MeCCMe)]$ (eq 3).

$$[W_2(Ot\text{-}Bu)_6] + RCCR \rightarrow 2[(t\text{-}BuO)_3WCR], \quad R = \text{alkyl} \tag{1}$$

$$5[Mo_3(\mu_3\text{-}CMe)_2(\mu\text{-}O_2CMe)_6(H_2O)_3]^{2+} + 2H_2O \rightarrow 4[Mo_3(\mu_3\text{-}CMe)_2(\mu\text{-}O_2CMe)_6(H_2O)_3]^{+} + [Mo_3(\mu_3\text{-}O)_2(\mu\text{-}O_2CMe)_6(H_2O)_3]^{2+} + MeCCMe + 4H^+ \tag{2}$$

$$[Mo_3(\mu_3\text{-}CMe)_2(\mu\text{-}O_2CMe)_6(H_2O)_3]^{2+} + 7Br^- \rightarrow [Mo_3(\mu_3\text{-}Br)(\mu\text{-}Br)_2Br_4(\mu\text{-}O_2CMe)(H_2O)_2(\mu_3\text{-}\eta_2\text{-}MeCCMe)] + H_2O + 5MeCOO^- \tag{3}$$

These results spark a rebirth of interest into the scarcely researched field of aqueous organometallic chemistry of high-valent metal complexes and cluster-based coupling and metathesis catalysts. In view of these findings, the triangulo perhaloclusters acquire special interest as suitable halide-based synthons for a meaningful systematic study of their reactions with alkynes.

Herein we report the isolation of the $[Mo_3(\mu_3\text{-}Br)_2(\mu\text{-}Br)_3Br_6]^{2-}$ (**1**, $\{Mo_3\}^{9+}$, 9 d-electrons) cluster, and we describe its structural and spectroscopic characterization along with computational studies. Moreover, density functional calculations are employed for the investigation of the electronic properties of the cluster. Our results support the description of the trimolybdenum core under the prism of three strongly antiferromagnetically coupled metals.

Experimental Section

All operations were performed anaerobically under a pure dinitrogen or argon atmosphere using Schlenk techniques on an inert gas/vacuum manifold or in a drybox (O_2, H_2O < 1 ppm). Starting materials were purchased from Sigma-Aldrich and are of the highest available purities. Tetrahydrofuran (THF) and diethyl ether were distilled over Na/Ph_2CO, MeCN, and PhCl over CaH_2 in an inert atmosphere. Solvents were degassed by three freeze−pump−thaw cycles. Nujol paraffin oil used for far-IR measurements was dried over Na. $(n\text{-}Bu)_4NBr$ was purified by recrystallization from acetone.[15] FT-IR spectra were obtained on Nicolet Nexus 470, 670, and Magna 750 spectrometers. UV−vis spectra were obtained on a Varian Cary 50 spectrophotometer. Microanalyses were done by Galbraith Laboratories, Knoxville, TN.

Cyclic voltammetry was carried out with an Eco Chemie Autolab PGSTAT100 electrochemical workstation fitted in a Drybox and controlled with a General Purpose Electrochemical Software (GPES). Cyclic voltammetry was performed using a gold disk working electrode (1.6 mm diameter) and a Ag/Ag^+ (0.01 M $AgNO_3$ and 0.1 M $(n\text{-}Bu)_4NPF_6$ in MeCN) non-aqueous reference electrode (Bioanalytical Systems, Inc.) with a prolonged bridge (0.1 M $(n\text{-}Bu)_4NPF_6$ in MeCN). A thin Pt gauge (8 cm^2, Sigma-Aldrich) was employed as counter electrode. The working electrode was polished using successively 6, 3, 1 μm diamond paste on a DP-Nap polishing cloth (Struers, Westlake, OH), washed with water, acetone, and air-dried. The Pt foil and gauge electrodes were cleaned in a H_2O_2/H_2SO_4(conc) solution (1/4 v/v) and oven-dried. The concentration of the samples was 3 mM and that of $(n\text{-}Bu)_4NPF_6$ (supporting electrolyte) was 0.1 M. The potential sweep rate varied between 20−1000 mV/s. All voltammograms were compensated for the solution resistance. All potentials are reported versus the ferrocenium/ferrocene (Fc^+/Fc) couple.

Mass spectrometric analyses were done using electrospray ionization on a Thermo-Finnigan TSQ7000 triple-quadrupole. The heated inlet capillary was kept at 250 °C, and the electrospray needle voltage was 4.5 kV. All other voltages were optimized to maximize ion transmission and minimize unwanted fragmentation and were determined during the regular tuning and calibration of the instrument. Nitrogen sheath gas was supplied to the electrospray source at 80 psi.

(4) (a) Chisholm, M. H.; Folting, K.; Huffman, J. C.; Kirkpatrick, C. C. *Inorg. Chem.* **1984**, *23*, 1021–1037. (b) Chisholm, M. H.; Folting, K.; Huffman, J. C.; Kirkpatrick, C. C. *J. Am. Chem. Soc.* **1981**, *103*, 5967–5968. (c) Chisholm, M. H.; Folting, K.; Huffman, J. C.; Kober, E. M. *Inorg. Chem.* **1985**, *24*, 241–245.
(5) Blatchford, T. P.; McCarley, R. E. *Chem. Abstr.* **1987**, *193*, 363.
(6) Spitsyn, V. I.; Kazin, P. E.; Felin, M. G.; Subbotina, N. A.; Zhirov, A. I.; Zelentsov, V. V. *Russ. J. Inorg. Chem.* **1987**, *32*, 1395–1397.
(7) Fettinger, J. C.; Gordon, J. C.; Mattamana, S. P.; O'Connor, C. J.; Poli, R.; Salem, G. *Inorg. Chem.* **1996**, *35*, 7404–7412.
(8) Cotton, F. A.; Poli, R. *J. Am. Chem. Soc.* **1988**, *110*, 830–841.
(9) Maoyu, S.; Jinling, H.; Jiaxi, L. *Jiegou Huaxue* (*J. Struct. Chem.*) **1984**, *3*, 13–16.
(10) Delphin, W. H.; Wentworth, R. A. D.; Matson, M. S. *Inorg. Chem.* **1974**, *13*, 2552–2555.
(11) Cavigliasso, G.; Stranger, R. *Inorg. Chem.* **2008**, *47*, 3072–3083.
(12) Zaera, F. *Chem. Rev.* **1995**, *95*, 2651–2693.
(13) (a) Schrock, R. R.; Listemann, M. L.; Sturgeoff, L. G. *J. Am. Chem. Soc.* **1982**, *104*, 4291–4293. (b) Listemann, M. L.; Schrock, R. R. *Organometallics* **1985**, *4*, 74–83.
(14) Bino, A.; Ardon, M.; Shirman, E. *Science* **2005**, *308*, 234–235.
(15) Perrin, D. D.; Armarego, W. L. F. *Purification of Laboratory Chemicals*, 3rd ed.; Pergamon Press: Oxford, U.K., 1989.

Samples were infused into the source at a rate of 10 μL/min using a 500 μL Gastight syringe (Hamilton, Reno, NV) in a Pump 11 syringe pump (Harvard Apparatus, Holliston, MA). Mass spectra were recorded with a scan range of m/z 200−2000 for positive and negative ions.

X-band electron paramagnetic resonance (EPR) spectra were recorded with an ER-200D Bruker spectrometer equipped with an Oxford ESR-9 cryostat, an Anritsu microwave frequency counter, and a Bruker NMR Gaussmeter. The Signal-Channel unit was replaced with an SR830 digital lock-in amplifier from Stanford Research. Magnetic susceptibility data were collected in the temperature range 2−300 K with a magnetic applied field of 0.5 T on a polycrystalline sample of the title compound (mass = 35.53 mg) with a Quantum Design MPMS-XL-5 SQUID magnetometer. The isothermal magnetization was measured on the same sample at 2 K with magnetic fields up to 5 T. The susceptibility data were corrected for the sample holder previously measured using the same conditions and for the diamagnetic contributions of the salt as deduced by using Pascal's constant tables ($\chi_{dia} = -740.6$ emu.mol^{-1}).

Crystallographic data were collected at the Department of Chemistry and Biochemistry at the University of Missouri-St. Louis using a Bruker SMART CCD (charge coupled device) based diffractometer equipped with an Oxford Cryostream low-temperature apparatus operating at variable low temperatures. A suitable crystal was chosen and mounted on a glass fiber using grease. Data were measured using omega scans of 0.3° per frame for 30 s, such that a hemisphere was collected. A total of 1271 frames were collected with a maximum resolution of 0.75 Å. The first 50 frames were recollected at the end of data collection to monitor for decay. Cell parameters were retrieved using SMART software and refined using SAINT on all observed reflections. Data reduction was performed using the SAINT software, which corrects for Lp and decay. The structures are solved by the direct method using the SHELXS-97 program and refined by the least-squares method on F^2, SHELXL-97, incorporated in SHELXTL-PC V 5.10. All non-hydrogen atoms were refined anisotropically. Hydrogens were calculated by geometrical methods and refined as a riding model. The crystals used for diffraction studies showed no decomposition during data collection. Drawings are done at 50% ellipsoids.

Synthesis of $[(n\text{-Bu})_4N]_2[Mo_3(\mu_3\text{-Br})_2(\mu\text{-Br})_3Br_6]$ (1). $[Mo(CO)_6]$ (0.462 g, 1.75 mmol) and $(n\text{-Bu})_4NBr$ (0.509 g, 1.75 mmol) were added in a Schlenk flask and were deoxygenated. PhCl (10 mL) was then added, and a reflux condenser equipped with a silicon trap was adjusted to the system. The reaction mixture was refluxed for 15 min. After cooling to room temperature, 1,2-$C_2H_4Br_2$ (5 mL) was added in small portions over a period of 10 min under continuous stirring. The reaction mixture was refluxed for 5 h, and then it was allowed to cool to room temperature. Addition of Et_2O (30 mL) afforded a green-brown solid, which was filtered, washed with Et_2O (2 × 10 mL), and dried under vacuum. Subsequently, the solid was dissolved in MeCN (7 mL), filtered, and the filtrate was dried. The residue was redissolved in MeCN (5 mL) and was kept in the refrigerator overnight to afford dark green crystals of **1** (98.5 mg, 10%). IR (KBr): 2962 (s), 2873 (s), 1462 (s), 1381 (s), 1280, 1262, 1163, 1031, 881, 799, 739 cm^{-1}. far-IR (Nujol): 278 (m/br), 235 (m/br), 181 (m) cm^{-1}. UV−vis (MeCN): λ_{max} (ε) 284 (27466), 312 (27766), 580 (541), 757 (147) nm (M^{-1} cm^{-1}). ESI-MS: m/z 415.57 ($[MoBr_4]^-$), 496.49 ($[MoBr_5]^-$), 584.5 ($[Mo_3Br_{11}]^{2-}$), 671.32 ($[Mo_2Br_6]^-$), 752.30 ($[Mo_2Br_7]^-$), 928.24 ($[Mo_3Br_8]^-$), 1087.05 ($[Mo_3Br_{10}]^-$), 1128.03 ($[Mo_3Br_{10}(MeCN)]^-$), 1409.34 ($[(n\text{-Bu})_4NMo_3Br_{11}]^-$). Anal. Calcd for $C_{32}H_{72}N_2Mo_3Br_{11}$: C, 23.27; H, 4.39; N, 1.70. Found: C, 23.12; H, 4.51; N, 1.75.

The corresponding Et_4N^+ and Et_3BzN^+ salts were crystallized from saturated MeCN or THF solutions, by dissolving **1** and a 2-fold excess of Et_4NCl and Et_3BzNCl, respectively.

Computational Details. Ground-state electronic structure calculations of complex **1** have been performed using density functional theory (DFT)[16] methods with the aid of the ORCA program package.[17] First, the geometry optimization was carried out under no symmetry constraint at the B3LYP[18,19] level of theory starting from the X-ray data. For both molybdenum and bromine atoms the polarized valence triple-ζ quality TZVP basis set developed by the Ahlrichs group[20,21] has been employed along with the related auxiliary basis set.[22] Scalar relativistic corrections were also included using the standard second-order Douglas−Kroll−Hess method. The optimum structure located as a stationary point on the potential energy surface was verified by the absence of imaginary frequencies. Non-relativistic single-point calculations on the optimized geometry were carried out to describe the ground state electron density of the complex under study. These calculations employed the B3LYP/TZVP combination and made use of the broken-symmetry (BS) formalism proposed by Ginsberg[23] and Noodleman.[24] Moreover, the nature of the solution was investigated from the point of view of the corresponding orbital transformation (COT).[25] According to this transformation, which is based on the corresponding orbital overlaps, the MOs are separated into three groups: (a) the group of MOs with spatial overlap essentially equal to unity, which can be considered as doubly occupied; (b) the group of MOs with spatial overlap significantly different from zero or unity, which form the valence bond like overlapping magnetic pairs of the BS solutions; and (c) the group of spin-up MOs that are unmatched by spin-down MOs because there are (for a state with $M_s > 0$) more a- than b-electrons in the system and that correspond to the singly occupied molecular orbitals (SOMOs) of the system. The graphics presented here were drawn with the aid of ChemCraft[26] and Molekel.[27,28]

Results and Discussion

Synthesis and Characterization. During our attempts to synthesize the heterobimetallic complex $[(n\text{-Bu})_4N]_2[MoW(\mu\text{-Br})_3(\mu\text{-Br})_6]$ $[(Mo\overset{2.5}{-}W)^{7+}, a'^2e'^3]$ from the reaction of equimolar amounts of $[Mo(CO)_6]$ and $[W(CO)_6]$ with 1,2-dibromoethane in boiling chlorobenzene, paralleling McCarley's synthesis of $[(n\text{-Bu})_4N]_2[W_2(\mu\text{-Br})_3(\mu\text{-Br})_6]$,[29] we have isolated from the reaction mixture a green trimolybdenum bromo complex (as evidenced by electrospray ionization mass spectrometry

(16) Parr, R. G.; Yang, W. *Density Functional Theory of Atoms and Molecules*; Oxford University Press: New York, 1989.
(17) Neese F. *ORCA - An ab initio, DFT and semiempirical SCF-MO Package*, Version 2.6, Revision 71; Max-Planck-Institut für Bioanorganische Chemie: Mülheim, Germany, 2005.
(18) Becke, A. D. *J. Chem. Phys.* **1993**, *98*, 5648–5652.
(19) Lee, C.; Yang, W.; Parr, R. G. *Phys. Rev. B* **1988**, *37*, 785–789.
(20) Schäfer, A.; Horn, H.; Ahlrichs, R. *J. Chem. Phys.* **1992**, *97*, 2571–2577.
(21) Schäfer, A.; Huber, C.; Ahlrichs, R. *J. Chem. Phys.* **1994**, *100*, 5829–5835.
(22) Weigend, F.; Häser, M. *Theor. Chem. Acc.* **1997**, *97*, 331–340.
(23) Ginsberg, A. P. *J. Am. Chem. Soc.* **1980**, *102*, 111–117.
(24) Noodleman, L. *J. Chem. Phys.* **1981**, *74*, 5737–5543.
(25) Neese, F. *J. Phys. Chem. Solids* **2004**, *65*, 781–785.
(26) Zhurko, G. A.; Zhurko, D. A. *ChemCraft, Tool for treatment of the chemical data*, version 1.6; www.chemcraftprog.com.
(27) Flükiger, P.; Lüthi, H. P.; Portman, S.; Weber, J. *MOLEKEL*, version 4.3; Swiss Center for Scientific Computing: Manno, Switzerland, 2000−2002.
(28) Portmann, S.; Luthi, H. P. *Chimia* **2000**, *54*, 766–770.
(29) Templeton, J. L.; Jacobson, R. A.; McCarley, R. E. *Inorg. Chem.* **1977**, *16*, 3320–3328.

(ESI-MS)) in minute quantities. Repeating the reaction with $[Mo(CO)_6]$ alone as starting material yielded larger quantities of the same compound (yield ~ 10%), along with the dinuclear complex $[(n\text{-}Bu)_4N]_2[Mo_2(\mu\text{-}Br)_3Br_6]$ (identified by ESI-MS and UV−vis spectroscopies; yield 65%). The trimetallic cluster proved to be $[(n\text{-}Bu)_4N]_2[Mo_3(\mu_3\text{-}Br)_2(\mu\text{-}Br)_3Br_6]$ (**1**). The $(n\text{-}Bu)_4N^+$ cation can be further replaced by Et_4N^+ and Et_3BzN^+ cations to generate the corresponding salts, by dissolving **1** in MeCN or THF and adding the chloride salt of these bulky cations. Complex **1** is stable in the solid state and in solution, and was fully characterized by elemental analysis, UV−vis, infrared spectroscopy, ESI-MS, and cyclic voltammetry.

Crystal Structure. The X-ray crystal structure of $[Mo_3(\mu_3\text{-}Br)_2(\mu\text{-}Br)_3Br_6]^{2-}$ was determined for all three ammonium salts noted above, after crystallization from MeCN and THF. Tetraphenylphosphonium salts proved to be oily and not suitable for single-crystal X-ray diffraction analysis. Significant disorder was encountered in all structure determination attempts of these salts to a different degree. Notably, severe structural disorder was previously reported for the iodo congener,[7] affecting both the cationic and anionic counterparts and suggesting an intrinsic problem with the structural determination of this type of clusters. We report here the structure of **1** from MeCN, which is the least disordered and best behaved of all resolved structures. Figure 1 depicts the thermal ellipsoid plot and the atom labeling scheme, and Table 1 lists the crystallographic data, whereas important bond lengths and angles are given in Table 2. The compound features an isosceles triangular core, related by a 2-fold axis that penetrates atom Mo(2), the midpoint of Mo(1)−Mo(1)#1 and atom Br(3). Two of the Mo(1, #1)−Mo(2) bonds are equidistant (2.7232(14) Å), while the third one displays a slight elongation (Mo(1)−Mo(1)#1 = 2.7702(18) Å), with an average value of 2.74 Å. Although the two Mo−Mo distances differ by only 0.05 Å, the metrical parameters and electronic properties (vide infra) of **1** show that this small difference cannot be overlooked. Two bromine atoms, related by the 2-fold axis, cap the Mo_3 triangle (Br(2) = Br_c, above and below), so that the $\{Mo_3(\mu_3\text{-}Br_c)_2\}$ set of atoms defines a distorted trigonal bipyramid. Three bromine atoms (Br(1), Br(#1), and Br(3) = Br_{br}) bridge each of the Mo−Mo edges (average Br_{br}−Mo−Br_{br} and Mo−Br_{br}−Mo angles are 175.50° and 64.44° respectively), forming an external isosceles triangle (Br(1,#1)−Br(3) = 5.135 Å, Br(1)−Br(1)#1 = 5.128 Å) coplanar to the Mo_3 core. Finally, six terminal bromine atoms (Br(4), Br(5), Br(6) and their symmetry related atoms Br(#4), Br(#5), and Br(#6) = Br_t) complete the total structure (average Mo−Br_t distance is 2.50 Å), affording a nine-electron trimetallic core. This bonding assembly, involving three group 6 metals both bridged and capped and containing six- and eight-electron cores ($\{Mo_3\}^{n+}$, n = 12, 10) is well established in the literature,[30,31] in contrast to the nine-electron clusters that are not so common.

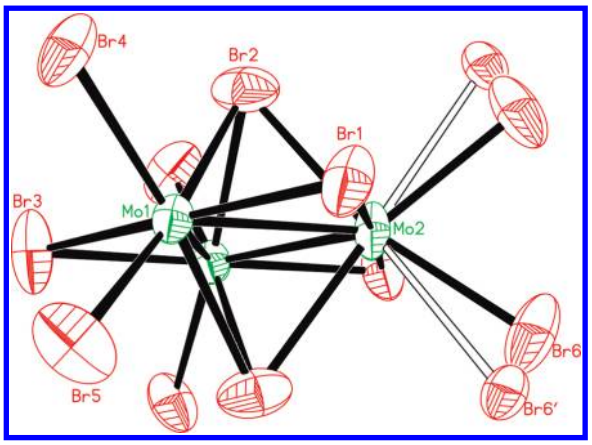

Figure 1. Solid-state structure of $[(n\text{-}Bu)_4N]_2[Mo_3(\mu_3\text{-}Br)_2(\mu\text{-}Br)_3Br_6]$ (**1**) showing 50% probability ellipsoids and the atom labeling scheme.

Table 1. Summary of the Crystallographic Data for **1**

formula	$C_{32}H_{72}Br_{11}Mo_3N_2$
M_r	1651.75
crystal system	monoclinic
space group	$C2/c$
a (Å)	20.077(2)
b (Å)	11.864(1)
c (Å)	22.521(2)
α (deg)	90
β (deg)	109.348(4)
γ (deg)	90
V (Å^3)	5061.3(9)
Z	4
D_{calcd} (g cm^{-3})	2.168
T (K)	100(2)
λ (Å)	0.71073
μ (mm^{-1})	9.440
$R_1{}^a(I > 2\sigma(I))$	0.0680
$wR_2{}^b(I > 2\sigma(I))$	0.1665

$^a R_1 = \sum||F_o| - |F_c||/\sum|F_o|$. $^b wR_2 = [\sum w(F_o{}^2 - F_c{}^2)^2/\sum w(F_o{}^2)^2]^{1/2}$.

Table 2. Selected Bond Lengths (Å) and Angles (deg) for **1** (Calculated and Experimental Values)

structural index	experimental values	calculated values
Mo(1)−Mo(2)	2.7232(14)	2.628
Mo(1)−Mo(1)#1	2.7702(18)	2.673
Mo(1)−Br(5)	2.5344(17)	2.613
Mo(1)−Br(4)	2.5227(15)	2.610
Mo(2)−Br(6)	2.432(3)	2.607
Mo(2)−Br(1)	2.5652(13)	2.662
Mo(1)−Br(1)	2.5655(15)	2.652
Mo(1)−Br(3)	2.5747(17)	2.644
Mo(2)−Br(2)	2.5811(17)	2.705
Mo(1)−Br(2)#1	2.5638(16)	2.676
Mo(1)−Br(2)	2.5662(17)	2.679
Mo(1)−Mo(2)−Mo(1)#1	61.14(5)	61.2
Mo(2)−Mo(1)−Mo(1)#1	59.43(2)	59.4
Mo(1)−Br(1)−Mo(2)	64.12(4)	59.2
Mo(1)−Br(3)−Mo(1)#1	65.09(6)	60.7
Br(1)−Mo(1)−Br(3)	174.73(5)	179.3
Br(1)−Mo(2)−Br(1)#1	177.04(7)	178.3
Br(4)−Mo(1)−Br(5)	86.86(6)	84.2
improper torsion[a]	51.7(7)	54.8

[a] This is the Br(2)−Mo(2)−X angle, where X is the projection of the Br(2) atom on the Mo_3 plane.

The trimetallic core, as well as the external triangle defined by the three bridging bromine atoms, satisfies a C_{2v} symmetry. The existence of the capping and terminal ligands forces the structure to drift along one of the C_2

(30) Müller, A.; Jostes, R.; Cotton, F. A. *Angew. Chem., Int. Ed. Engl.* **1980**, *19*, 875–882.
(31) Jiang, Y.; Tang, A.; Hoffmann, R.; Huang, J.; Lu, J. *Organometallics* **1985**, *4*, 27–34.

Table 3. Peaks Observed in the ESI-MS Spectrum of **1**

m/*z* experimental	*m*/*z* calculated	fragment
415.57	416	$[MoBr_4]^-$
496.49	497	$[MoBr_5]^-$
584.51	584.5	$[Mo_3Br_{11}]^{2-}$
671.32	672	$[Mo_2Br_6]^-$
752.30	753	$[Mo_2Br_7]^-$
928.24	928	$[Mo_3Br_8]^-$
1087.05	1088	$[Mo_3Br_{10}]^-$
1128.03	1129	$[Mo_3Br_{10}(MeCN)]^-$
1409.34	1411	$[(n\text{-}Bu)_4NMo_3Br_{11}]^-$

axes, with the deviation being more prominent in the Mo−Br_t distances. This slight, but not insignificant, deviation breaks the symmetry of the molecule leading the cluster to its final C_2 total symmetry. Deviations from a highly symmetric structure are also observed in relevant $\{Mo_3\}^{9+}$ clusters reported in the literature.[32]

Electrospray Ionization Mass Spectrometry. ESI-MS was additionally used for the characterization of **1**. The experimental isotope clusters obtained are in agreement with the theoretical masses and isotope patterns. The parent ion multiplet $[(n\text{-}Bu)_4NMo_3Br_{11}]^-$ was observed in the mass spectrum, along with signals attributed to di- or mononuclear fragments, as shown in Table 3.

Electrochemistry. Cyclic voltammetry experiments of **1** in MeCN show a chemically and kinetically reversible oxidation wave at $E_{1/2} = -0.892$ V versus the Fc^+/Fc couple ($\Delta E = 63$ mV, $i_{p,a}/i_{p,c} = 1.08$) and an irreversible reduction wave at $E_{p\text{-}c} = -1.623$ V (vs Fc^+/Fc). This behavior was maintained for scan rates ranging from 20 mV/s to 1000 mV/s (the ΔE and $i_{p,a}/i_{p,c}$ values given above are taken from voltammograms recorded at 100 mV/s, Figure 2, left). Randles−Sevcik plots yielded straight lines, indicating diffusion controlled processes (Figure 2, left, inset). Voltammograms of the oxidation wave normalized by dividing the faradaic current by the square root of the potential sweep rate are superimposable over a wide range of sweep rates, confirming its full chemical and kinetic reversibility (Figure 2, right).

The electrochemical data indicate that **1** undergoes a facile one-electron oxidation at easily accessible potentials with retention of its structure. The reversible Mo_3^{9+}/Mo_3^{10+} transformation is well documented in the literature.[32a,33,34] Reduction of **1** yields an unstable unidentified product and is therefore irreversible.

Electronic Structure. The UV−vis spectrum of **1** (MeCN solution, Figure 3) exhibits maxima at 284 (27500), 312 (27800), 580 (500), 757 (150), 919 (50) nm (M^{-1} cm^{-1}). Compound **1** is paramagnetic, and the EPR spectrum at room temperature consists of a rhombic signal with $g_1 = 2.077$, $g_2 = 1.950$, $g_3 = 1.770$ consistent with an anisotropic $S = 1/2$ system (Figure 4). Moreover, the isotropic value $g_{iso} = [(g_1 + g_2 + g_3)/3]$ is 1.93 (< 2), as expected for one Mo(III) ion. The spectrum is similar to that reported earlier for compound $[Mo_3(\mu_3\text{-}O)(\mu\text{-}Cl)_3(OAc)_3Cl(PMe_3)_2]$,[32a] which also contains a $\{Mo_3\}^{9+}$ core, and is consistent with the presence of one unpaired electron (see magnetic properties below).

Magnetic Susceptibility Measurements. The product of the molar magnetic susceptibility times the temperature ($\chi_m T$, proportional to μ_{eff}) shows a constant value of about 0.30 emu K mol^{-1} at room temperature, corresponding to an effective magnetic moment, $\mu_{eff} = 1.55\,\mu_B$. This value is significantly lower than the value expected for three non-interacting Mo(III) ions ($3\,\mu_B$), and is closer to the spin-only value ($1.73\,\mu_B$) for $S = 1/2$ systems. When the temperature is decreased, the $\chi_m T$ product remains almost constant down to about 50 K. At lower temperatures $\chi_m T$ shows a smooth decrease to reach a value of about 0.25 emu K mol^{-1} at 2 K (Figure 5). This behavior indicates that the trimolybdenum cluster exhibits strong antiferromagnetic interactions, and in the 2−300 K temperature range only the $S = 1/2$ states are occupied (see Supporting Information; pp S3, S4). The smooth decrease observed at low temperatures can be attributed to the presence of weak intercluster antiferromagnetic interactions (thanks to the extended bromide orbitals) and/or to the presence of a spin−orbit coupling, as has been previously reported for Mo(III) halide compounds.[10,11,32a,35] To simulate this magnetic behavior we have assumed that these intercluster interactions are isotropic and weak and, therefore, that compound **1** can be considered as a $S = 1/2$ paramagnet with a weak intercluster magnetic coupling that can be reproduced with the molecular field approximation.[36] This simple model reproduces very satisfactorily the magnetic properties of compound **1** with $g = 1.7786(6)$ and $J = -5.2(1)$ cm^{-1} (solid line in Figure 5). As expected, the g value is well below the theoretical value, since the magnetic moment is lower than expected because of the spin−orbit coupling present in the trimolybdenum complex. Note that the J value obtained (assuming eight nearest neighbors around each trimolybdenum cluster) is higher than expected, suggesting that the spin−orbit coupling is also included in this effective J value.

An additional proof of the weak intercluster antiferromagnetic coupling comes from the isothermal magnetization at 2 K that shows a saturation value slightly below 1 μ_B, which is the expected value for an $S = 1/2$ paramagnet. Thus, the magnetization data can be quite well reproduced with the simple Brillouin function for an $S = 1/2$ system with a reduced g value of 1.590(4) (inset in Figure 5).

Computational Studies. Cluster **1** possesses an almost C_2 total geometry in space. Nevertheless, the trimetallic core could be envisioned as if it consists of three mononuclear interpenetrating bicapped octahedra. In each of them, the molybdenum central atom is ligated through six bromine atoms that form the main distorted octahedral environment (two terminal, two bridging, and two capping). The other two molybdenum atoms of the

(32) (a) Cotton, F. A.; Shang, M.; Sun, Z. S. *J. Am. Chem. Soc.* **1991**, *113*, 6917–6922. (b) Cotton, F. A.; Shang, M.; Sun, Z. S. *J. Clust. Sci.* **1992**, *3*, 123–144. (c) Cotton, F. A.; Shang, M.; Sun, Z. S. *Inorg. Chim. Acta* **1993**, *212*, 95–104.

(33) (a) Cotton, F. A.; Shang, M.; Sun, Z. S. *J. Am. Chem. Soc.* **1991**, *113*, 3007–3011. (b) Cotton, F. A.; Shang, M.; Sun, Z. S. *J. Clust. Sci.* **1992**, *3*, 109–121.

(34) Qiu-Hua, C.; Shao-Fang, L.; Jian-Quan, H.; Zi-Xiang, H.; Xiao-Ying, H. *Jiegou Huaxue* (*Chinese J. Struct. Chem.*) **1993**, *12*, 117–123.

(35) Mironov, V. S.; Chibotaru, L. F.; Ceulemans, A. *J. Am. Chem. Soc.* **2003**, *125*, 9750–9760.

(36) O'Connor, C. J. *Prog. Inorg. Chem.* **1982**, *29*, 203.

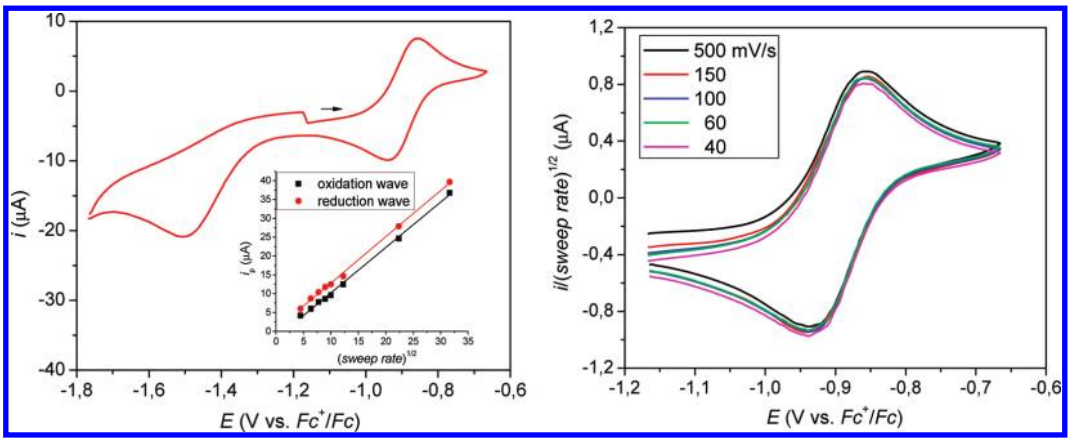

Figure 2. Left: Cyclic voltammetry of **1** (3.0 mM) in MeCN/0.1 M $(n\text{-Bu})_4NPF_6$ with a Au-disk electrode (1.6 mm in diameter); scan rate 100 mV/s. Arrow indicates the direction of scan. Inset: Randles−Sevcik plots for the anodic part of the oxidation wave and the cathodic part of the reduction wave. Right: Plots of $i/(sweep\ rate)^{1/2}$ versus E (oxidation wave) for various sweep rates, as indicated. The experiments were carried out in a drybox under nitrogen.

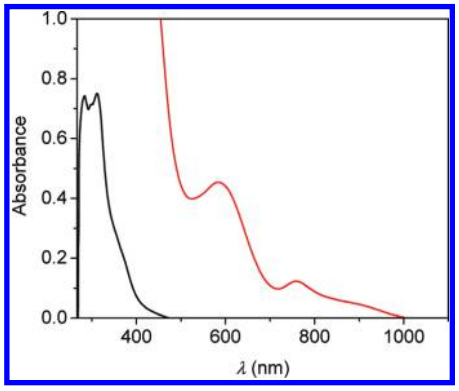

Figure 3. UV−vis spectrum of **1** (2.7×10^{-5} M, black line; 8.4×10^{-4} M, red line) in MeCN.

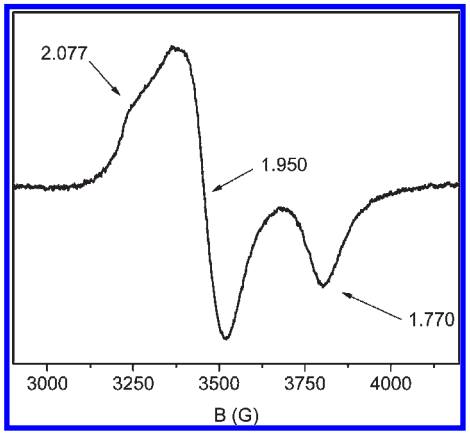

Figure 4. EPR spectrum of **1** (solid) at room temperature. EPR conditions: modulation amplitude 1 Gpp; microwave power 55 mW; microwave frequency 9.4255 GHz.

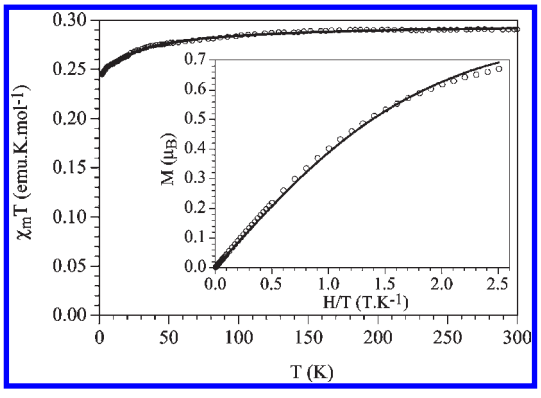

Figure 5. Thermal variation of the $\chi_m T$ product for **1**. Inset shows the isothermal magnetization at 2 K. Solid lines are the best fit to the models (see text).

trimetallic cluster act as capping ligands in the octahedron triangular faces (determined by the two μ_3- and one μ-bromine ligands). The relatively compact structure causes the octahedra to be distorted. As a result, the Mo−Br_t and Mo−Br_c bonds bend out of the triangular core.

Each molybdenum center in its octahedral environment is described as a formal Mo(III) cation with a d^3 (t_{2g}^3) electron configuration. Under the framework of group theory arguments (with the z-axis for every Mo atom pointed toward the center of the triangle and the x-axis lying on the triangle plane), the symmetry adapted linear combinations (SALCs) of the three sets of t_{2g} fragment orbitals transform to $a_1' + e'$ (for z^2 and $x^2 - y^2$), $a_2'' + e''$ (for yz), $a_2' + e'$ (for xz), and $a_1'' + e''$ (for xy). As a result of the orbital interactions among these linear combinations, the first two sets are bonding, whereas the other two are antibonding. Preliminary DFT calculations on the Mo_3 core satisfying an equilateral triangle arrangement ($d = 2.75$ Å) predict that the first six of the nine electrons occupy the $3a_1'$ and $4e'$ bonding orbitals, with the next two occupying the $2a_2''$. Thus, the last electron should enter the antibonding $4a_1'$, with the ground state being $^2A_1'$. However, when the ligand cage is introduced, major changes are induced to the bonding scheme. The bonding d orbital combinations, which accommodate significant electron density toward incoming ligands, are anticipated to be greatly destabilized. This effect is enhanced by the capping ligands.[30,31,37] As a result, $a_1' + e'$ orbitals (z^2 combinations) should remain bonding, while $a_1'' + e''$ combination would become antibonding because of the interaction with the bromine

(37) Bursten, B. E.; Cotton, F. A.; Hall, M. B.; Najjar, R. C. *Inorg. Chem.* **1982**, *21*, 302–307.

π-donor bridging ligands. Similar is the case for $a_1' + e'$ ($x^2 - y^2$ combinations) and $a_2' + e'$ SALCs.

On the other hand, Cotton and Hoffmann, following the "clusters in molecules" approach[31,37,38] for structurally relevant clusters, concluded that the introduction of the ligands in the trinuclear cluster of pure D_{3h} would cause a significant Jahn−Teller distortion forcing the symmetry to be reduced toward the C_{2v} or the C_2 geometry through an e′ normal mode. According to this, in the case of complex **1**, the ideal trigonal biprismatic cluster is calculated to have a $^2E''$ ground state, and the SOMO orbital in our nine electron cluster is a doubly degenerate orbital, which is formed mainly by antibonding contributions among metal d_{yz} orbitals and bromine (bridging and terminal) p orbitals. Thus, an E′ normal mode, according to the point group theory arguments,[39] would break the symmetry of the main C_3 vertex leading to a stabilized Jahn−Teller structure of lower symmetry. Forwarding our discussion to the electronic properties of **1** (in the C_2 point group), the molecular orbitals scheme of an $S = 1/2$ cluster should resemble the following qualitative scheme: six bonding electrons residing in three symmetry adapted combinations of metal d orbitals of *a*- or *b*-symmetry and three additional electrons occupying one antibonding orbital and one essentially nonbonding orbital, with respect to Mo−Mo main cluster core bonds.

Cluster **1** has been fully geometry optimized under no symmetry constraint employing a polarized valence triple-ζ quality basis set. The main structural parameters obtained are summarized in Table 2. The calculated geometry is in good agreement with the experiment, with the major discrepancies located in the metal−metal distances, although the intermetallic distances are within the range anticipated for a metal−metal bond.

To elucidate the electronic structure of **1**, we employed the broken-symmetry (BS) formalism, as introduced by Ginsberg,[23] standardized by Noodleman,[24] and currently used often in the description of molecules with non-innocent electronic character.[40−60] We should point out that the broken-symmetry state is not a spin eigenfunction and thus a pure spin state of the system but rather a superposition of spin eigenfunctions, with their respective contributions given by properly weighted Clebsch−Gordan coefficients.[24] Under this framework, the cluster under study features three molybdenum metal centers in an isosceles triangular arrangement, with Mo(2) in the apex of the triangle and Mo(1) and Mo(3)-(≡Mo(1)#1) being equivalent. The states under study are described as a high spin state (↑↑↑) and two broken symmetry states, for example, BS2(↑↑↓) and BS1(↑↓↑). We should point out that a state with a configuration BS4(↓↑↑) should not be considered because of the C_2 axis of symmetry present. In a case like this, the Heisenberg−Dirac−van Vleck (HDVV) Hamiltonian takes the following form:[61]

$$\hat{H} = -2J_{12}(\hat{S}_1\hat{S}_2 + \hat{S}_2\hat{S}_3) - 2J_{13}\hat{S}_1\hat{S}_3 \qquad (4)$$

where J_{ij} is the exchange parameter between the centers *i* and *j*. A negative value corresponds to an antiferromagnetic interaction, while the state with the lowest spin multiplicity is expected to be the ground state.

Employing Kambe's vector coupling model,[62] the spin operators $\hat{S}^* = \hat{S}_1 + \hat{S}_3$ and $\hat{S}' = \hat{S}^* + \hat{S}_2$ can be introduced in eq 4, leading to the energies of the spin levels provided in eq 5 ($\hat{S}^* = 0$ and 1, $\hat{S}' = 3/2$ and 1/2).

$$E = -(J_{13} - J_{12})\hat{S}^*(\hat{S}^* + 1) - J_{12}\hat{S}'(\hat{S}' + 1) \qquad (5)$$

In this equation, the energy depends only on $\hat{S}^*$ and $\hat{S}'$.[61,63] On the basis of the calculated energies from our DFT results, we extract the values of coupling constants J_{ij}. Thus, $J_{12} = -404$ cm^{-1} and $J_{13} = -343$ cm^{-1} (see Supporting Information for details; p S2).

Within this framework, the lowest broken symmetry state anticipated exhibits total spin $S = 1/2$ with the apex of the triangle accommodating the spin-down electron. Figure 6 exhibits the qualitative molecular orbital scheme derived for **1** based on the corresponding orbital analysis in case of the BS1 solution (vide supra). According to our calculations the system has three metal-based SOMOs, two of which strongly interact antiferromagnetically with each other. From the latter two, the alpha electron resides on the triangle base, whereas the beta one is localized on the triangle apex. The low value of the spatial overlap ($S = 0.23$) is a signature of a spin coupled electron pair. The third electron is also located on the triangle base.

(38) Chisholm, M. H.; Cotton, F. A.; Fang, A.; Kober, E. M. *Inorg. Chem.* **1984**, *23*, 749–754.
(39) (a) Lin, Z.; Fan, M.-F. *Struct. Bonding* (*Berlin*) **1997**, *87*, 35–80. (b) Cotton, F. A. *Chemical Applications of Group Theory*; Wiley Interscience: New York, 1990.
(40) Bénard, M.; Berry, J. F.; Cotton, F. A.; Gaudin, C.; Lopez, X.; Murillo, C. A.; Rohmer, M. M. *Inorg. Chem.* **2006**, *45*, 3932–3940.
(41) Lopez, X.; Benard, M.; Rohmer, M.-M. *Inorg. Chem.* **2007**, *46*, 5–7.
(42) Delfs, C. D.; Stranger, R. *Inorg. Chem.* **2001**, *40*, 3061–3076.
(43) Petrie, S.; Stranger, R. *Inorg. Chem.* **2002**, *41*, 2341–2347.
(44) Stranger, R.; Petrie, S. *J. Chem. Soc., Dalton Trans.* **2002**, 3630–3639.
(45) Bachler, V.; Olbrich, G.; Neese, F.; Wieghardt, K. *Inorg. Chem.* **2002**, *41*, 4179–4193.
(46) Banerjee, A.; Singh, R.; Chopra, D.; Colacio, E.; Rajak, K. K. *J. Chem. Soc., Dalton Trans.* **2008**, 6539–6545.
(47) Bencini, A.; Totti, F. *J. Chem. Theory Comput.* **2009**, *5*, 144–154.
(48) Blanchard, S.; Neese, F.; Bothe, E.; Bill, E.; Weyhermuller, T.; Wieghardt, K. *Inorg. Chem.* **2005**, *44*, 3636–3656.
(49) Cavigliasso, G.; Lovell, T.; Stranger, R. *J. Chem. Soc., Dalton Trans.* **2006**, 2017–2025.
(50) Cavigliasso, G.; Stranger, R. *Inorg. Chem.* **2008**, *47*, 3072–3083.
(51) Chlopek, K.; Bothe, E.; Neese, F.; Weyhermuller, T.; Wieghardt, K. *Inorg. Chem.* **2006**, *45*, 6298–6307.
(52) Chlopek, K.; Muresan, N.; Neese, F.; Wieghardt, K. *Chem.—Eur. J.* **2007**, *13*, 8391–8403.
(53) Ghosh, M.; Weyhermuller, T.; Wieghardt, K. *J. Chem. Soc., Dalton Trans.* **2008**, 5149–5151.
(54) Herebian, D.; Wieghardt, K. E.; Neese, F. *J. Am. Chem. Soc.* **2003**, *125*, 10997–11005.
(55) Kirchner, B.; Wennmohs, F.; Ye, S. F.; Neese, F. *Curr. Opin. Chem. Biol.* **2007**, *11*, 134–141.
(56) Liu, I. P. C.; Lee, G. H.; Peng, S. M.; Benard, M.; Rohmer, M. M. *Inorg. Chem.* **2007**, *46*, 9602–9608.
(57) Muresan, N.; Chlopek, K.; Weyhermuller, T.; Neese, F.; Wieghardt, K. *Inorg. Chem.* **2007**, *46*, 5327–5337.
(58) Sinnecker, S.; Neese, F.; Lubitz, W. *J. Biol. Inorg. Chem.* **2005**, *10*, 231–238.
(59) Sinnecker, S.; Neese, F.; Noodleman, L.; Lubitz, W. *J. Am. Chem. Soc.* **2004**, *126*, 2613–2622.
(60) Zhang, Y. Q.; Luo, C. L. *J. Chem. Soc., Dalton Trans.* **2008**, 4575–4584.
(61) Mabbs, F. E.; Machin, D. J. *Magnetism and Transition Metal Complexes*; Dover Publications, Inc.: New York, 2008.
(62) Kambe, K. *J. Phys. Soc. Jpn.* **1950**, *5*, 48–51.
(63) Kahn, O. *Molecular Magnetism*; VCH: New York, 1993.

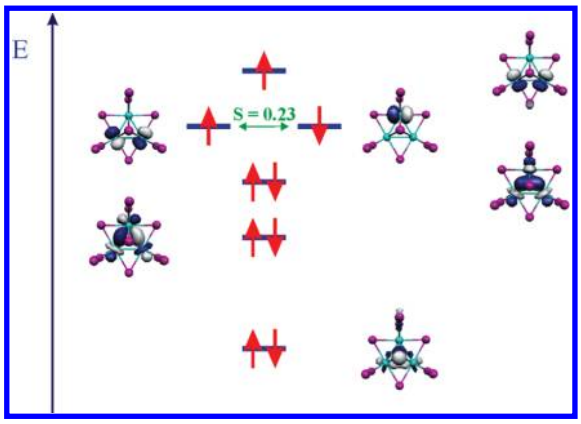

Figure 6. Qualitative molecular orbital diagram for **1** along with 0.05 au contour plots of the corresponding orbital analysis.

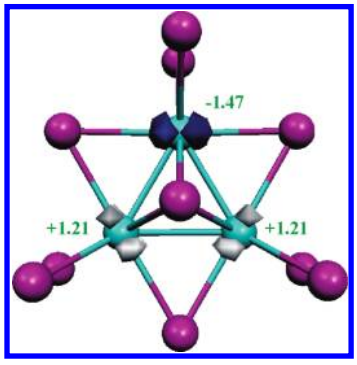

Figure 7. Spin density plot along with Mulliken spin population analysis for BS1.

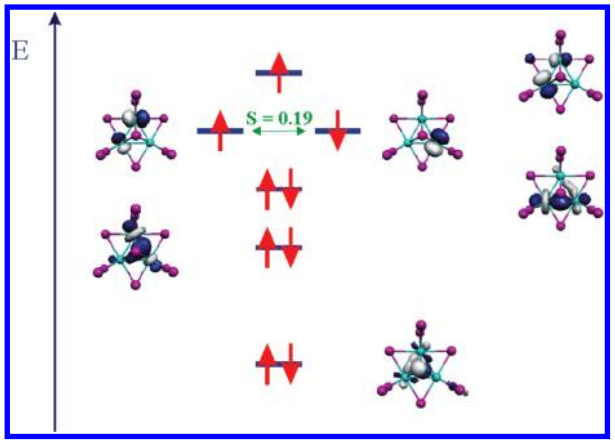

Figure 8. Qualitative molecular orbital diagram for BS2 along with 0.05 au contour plots of the corresponding orbital analysis.

The three relative molecular orbitals (two *a* and one *b*) span very close in energy, in a region of 0.05 eV forming a nearly degenerate group of orbitals. The occupied-unoccupied orbitals' gap was calculated to be 2.77 eV for the alpha manifold and 2.80 eV for the beta manifold. A spin population analysis is shown in Figure 7. Moreover, there are three orbitals having bonding interactions between metal centers, arising mainly from linear combinations of d orbitals. Two of them can be described owning *a*- and one having *b*-symmetry under the C_2 point group. The Mayer bond orders calculated for the metal−metal bonds yielded 0.81 and 0.88 for the base and apical bonds, respectively.

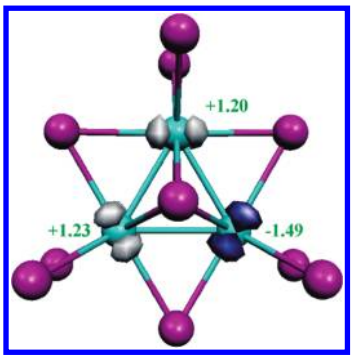

Figure 9. Spin density plot along with Mulliken spin population analysis for BS2.

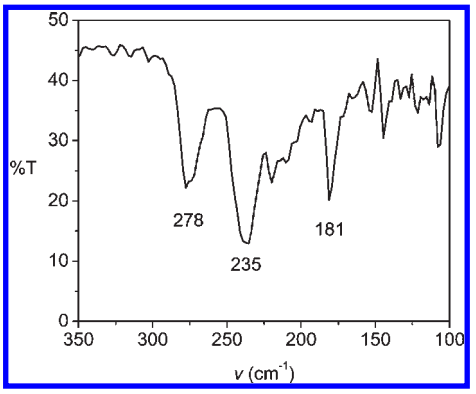

Figure 10. Far-IR spectrum of compound **1**.

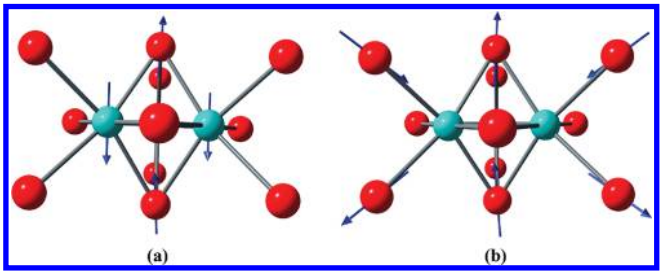

Figure 11. Graphical representations of two of the IR-active normal modes, responsible for the bands at 278 (a) and 181 (b) cm^{-1}.

The second broken symmetry state (BS2) found is lying only 0.4 kcal/mol (121 cm^{-1}) above BS1. In this conformation the beta electron resides in the triangle's base, while the spatial overlap is 0.19. In Figure 8 the relative qualitative molecular orbital diagram for the BS2 solution is depicted. A spin population analysis is shown in Figure 9.

From the aforementioned description it can be expected that at room temperature both broken symmetry states are populated; thus, the beta electron resides almost equally in each molybdenum site, and the antiferromagnetic character is delocalized over three magnetic orbitals populated by three electrons.

Vibrational Spectroscopy. The far-IR spectrum of **1** shows peaks at 278 (m/br), 235 (m/br), and 181 (m) cm^{-1} (Figure 10). For the 14-atom molecule $[Mo_3(\mu_3\text{-}Br)_2(\mu\text{-}Br)_3Br_6]^{2-}$, there are 36 overall degrees of freedom, all being IR active.

The mode assignments from our DFT calculations indicate that these modes have significant amplitude,

involving atoms in the metal core and in the bromine cage. Thus, the first peak (278 cm^{-1}) should be raised mainly by the asymmetric stretch of the $Mo-Br_c$ bonds, shown in Figure 11a. The second broadband according to our calculations contains two fundamentals that are raised by stretching modes regarding the $Mo-Br_t$ and $Mo-Br_{br}$ bonds. Finally, the band at 181 cm^{-1} should be raised by the asymmetric stretch of the $Mo-Br_t$ bonds, shown in Figure 11b.

Conclusions

The novel triangulo-perbromo-cluster $[(n\text{-}Bu)_4N]_2[Mo_3(\mu_3\text{-}Br)_2(\mu\text{-}Br)_3Br_6]$ (**1**, $\{Mo_3\}^{9+}$, 9 d electrons) has been isolated and characterized. Its crystal structure reveals a bicapped trigonal arrangement, where the three molybdenum centers are bridged by bromine atoms. Its spectroscopic and electrochemical properties, along with our DFT calculations indicate that its ground state is a doublet, with the three molybdenum atoms being strongly antiferromagnetically coupled. Our calculations are consistent with the irreversible reduction of **1** and the retention of the trimetallic core during its reversible one-electron oxidation procedure. The latter makes **1** a potent oxidant of organic substrates or an agent for charge transfer reactions. Moreover, our data under the broken symmetry formalism indicate that the antiferromagnetic character is delocalized over three magnetic orbitals populated by three electrons. Our current efforts focus on developing a synthetic strategy for its efficient preparation, which will permit the systematic study of its chemistry, especially reactions with alkynes, and the potential utility of the $\{Mo_3\}^{9+/10+}$ redox couple in stoichiometric or catalytic oxidations of organic substrates.

Acknowledgment. We acknowledge the Special Account for Research Grants of the University of Athens (70/4/3342), the NIH/NIEHS (5 P42 ES007381) grant, the European Union (MAGMANet and COST Action D35-WG-0011-05), the Spanish Ministerio de Educación y Ciencia (Projects MAT2007-61584 and CSD 2007-00010 Consolider-Ingenio in Molecular Nanoscience), and the Generalitat Valenciana (Project PROMETEO/2009/095) for financial assistance. We thank Prof. Nicholas Leventis for assistance with the electrochemical study, Dr. Nathan Leigh for obtaining the ESI-MS spectra, and Dr. Dimitris Maganas for assistance with the Orca package.

Supporting Information Available: X-ray crystallographic data for compound **1** in CIF format. Coordinates for DFT calculations (p. S1), eigenvalues of the spin-Hamiltonian $E(\hat{S}', \hat{S}^*)$ and DFT results for **1** (p. S2), and theoretical curves of the product χT over T for a system containing three interacting $S = 1/2$ spins (pp. S3, S4). This material is available free of charge via the Internet at http://pubs.acs.org.